

LHCHWG-2026-004
IFT-UAM/CSIC-26-65

NLO EW and QCD dimension-6 SMEFT results for Higgs and gauge boson decays in POPxf format

Luigi Bellafronte^{1*}, Sally Dawson^{2†}, Clara Del Pio^{2‡},
Matthew Forsslund^{3◦} and Pier Paolo Giardino^{4§}

¹ Physics Department, Florida State University, Tallahassee, FL 32306-4350, USA

² High Energy Theory Group, Physics Department, Brookhaven National Laboratory, Upton, NY 11973, USA

³ Princeton Center for Theoretical Science, Princeton University, Princeton, NJ, 08544 USA

⁴ Departamento de Física Teórica and Instituto de Física Teórica UAM/CSIC, Universidad Autónoma de Madrid, Cantoblanco, 28049, Madrid, Spain

* lbellafronte@fsu.edu, † dawson@bnl.gov, ‡ cdelpio@bnl.gov,
◦ mforsslund@princeton.edu, § pier.giardino@uam.es

Abstract

We present next-to-leading-order (NLO) QCD and electroweak (EW) results using the dimension-6 SMEFT for all 2- and 4- body Higgs decays, for Z and W decays along with the corresponding EW precision observables, and for the Higgstrahlung process $e^+e^- \rightarrow ZH$ at $\sqrt{s} = 240, 365$ and 500 GeV. The results are presented in the POPxf format for ease of use in experimental and phenomenological studies. Of particular utility is the total Higgs width, including all dimension-6 contributions at NLO. In addition, we present the differential distributions $d\Gamma/dm_{Z^*}$ for $H \rightarrow l^+l^-Z^*, Z^* \rightarrow l^+l^-$ at NLO in the SMEFT.

Copyright attribution to authors.

This work is a submission to SciPost Physics.

License information to appear upon publication.

Publication information to appear upon publication.

Received Date

Accepted Date

Published Date

Contents

1	Introduction	2
2	Processes	3
3	Results	4
3.1	Higgs Decays	4
3.2	Electroweak Observables	5
3.3	Higgstrahlung	7
4	Conclusion	7

1 Introduction

One of the major goals of the high-luminosity LHC is to precisely limit or to observe deviations from the Standard Model (SM) predictions. The Standard Model Effective Field Theory (SMEFT) [1] is a useful tool for searching for high scale new physics effects not present in the SM and postulates that there are no unobserved light particles and that the gauge symmetry remains the $SU(3) \times SU(2) \times U(1)$ symmetry of the SM. The Lagrangian is then expanded around the SM,

$$\mathcal{L} = \mathcal{L}_{SM} + \sum_{i,d} \frac{\hat{C}_i^{(d)}}{\Lambda^{d-4}} \mathcal{O}_i^{(d)}, \quad (1)$$

where $\mathcal{O}_i^{(d)}$ are the complete set of $SU(3) \times SU(2) \times U(1)$ invariant dimension- d operators constructed out of SM fields and $\hat{C}_i^{(d)}$ are the corresponding Wilson coefficients, which we take to be in the Warsaw basis [2, 3]. We restrict ourselves to dimension-6 operators. The expansion parameter, Λ , is assumed to be TeV scale or higher.

Predictions for physical observables, O_α , are expanded around the SM predictions as an inverse power series in Λ and in the loop expansion, $\frac{1}{16\pi^2}$,

$$O_\alpha = O_{\alpha,SM} + \sum_{i,j,d} \beta_{\alpha,i,j} \frac{\hat{C}_i^{(d)}}{(\Lambda^{d-4})(16\pi^2)^j} \quad (2)$$

Tree level observables ($j = 0$) accurate to dimension-6 ($d = 6$) can be computed in a straightforward manner using MADGRAPH [4] in conjunction with SMEFTsim [5] or SMEFT@NLO [6]. We retain terms only to $\mathcal{O}(\frac{1}{\Lambda^2})$ since a consistent tree level calculation to $\mathcal{O}(\frac{1}{\Lambda^4})$ would require including the contributions of dimension-8 operators.

The anticipated precision from the HL-LHC, along with projections for FCC-ee, require that the SMEFT predictions be computed beyond the leading order in the loop expansion. Next-to-leading-order (NLO) QCD corrections including the contributions of dimension-6 operators can be found from the automated tools listed above. NLO electroweak (EW) corrections, however, present a different challenge from QCD corrections, as they typically introduce a dependence on dozens of Wilson coefficients that do not contribute at tree level and are calculated on a case-by-case basis, with the results scattered through the literature. The NLO calculations we describe in this note are accurate to $\mathcal{O}(\frac{1}{16\pi^2\Lambda^2})$, as reaching the accuracy $\mathcal{O}(\frac{1}{16\pi^2\Lambda^4})$ would require the inclusion of one-loop diagrams with two insertions of dimension-6 operators, along with dimension-8 operators, which is beyond the scope of the results presented here.

The numerical results of the various existing dimension-6 NLO QCD/EW calculations can be conveniently summarized using the POPxf approach [7]. The POPxf exchange format is a recently proposed data structure designed to standardize arbitrary polynomial dependences of observables on model parameters to simplify sharing and reproducing theoretical predictions in effective field theory (EFT) analyses. The format supports observables expressed as arbitrary functions of polynomials of any degree, and also allows the inclusion of uncertainties and correlations. Additional metadata entries include all relevant information for reproducibility, including renormalization scales, parameter inputs, choice of SMEFT basis, etc.

Our usage of this formalism includes the numerical results for $\beta_{\alpha,i,0}$ and $\beta_{\alpha,i,1}$ in JSON files which include sufficient information such that the results can be replicated by the user. Our observables for Higgs decays consist of inclusive decay widths, branching ratios, and some differential distributions for $H \rightarrow 4\ell$ that will be discussed below. While the POPxf format allows arbitrary degree polynomials, to maintain a consistent power counting all our results are expanded only up to linear $\mathcal{O}(\frac{1}{\Lambda^2})$ order. In this note, we compile and present NLO results for Higgs decays [8, 9], W and Z decays along with the corresponding electroweak precision observables [10–12], and the Higgstrahlung process, $e^+e^- \rightarrow ZH$ [13, 14]. The POPxf files are located at a [GitLab](#) repository.

2 Processes

As described in [8, 9], all of the two- and four-body Higgs decays and branching ratios are now known to NLO QCD/EW in the dimension-6 SMEFT in the narrow width approximation:

$$H \rightarrow \gamma\gamma, \quad H \rightarrow \gamma Z, \quad H \rightarrow gg$$

$$H \rightarrow f\bar{f}, \quad f \in [b, \tau, \mu, c, s] \quad (3)$$

$$H \rightarrow (f_{g_1}\bar{f}_{g_1})(f_{g_2}\bar{f}_{g_2}), \quad f \in [\ell, \nu_\ell, u, d] \quad (4)$$

where $g_k = 1, 2, 3$ is a generation index. These processes are implemented in the public code NEWISH [15]. Our default set of input parameters for Higgs decays is $\{M_W, M_Z, G_F\}$. The couplings and gauge boson masses are renormalized in the on-shell scheme. We present results using both the on-shell and the $\overline{\text{MS}}$ renormalization scheme for fermion masses. All results have an arbitrary flavor scheme, which can easily be restricted to a desired flavor assumption. The results for the total Higgs decay widths, along with numerical values of the input parameters can be found in POPxf notation at the GitLab repository [16]. In addition, for the 4-body Higgs decays to leptons, we also include distributions for $H \rightarrow 4\ell$ in the GitLab repository.

The NLO QCD/EW dimension-6 results for Z and W decays have also been implemented in POPxf formalism in both the $\{M_W, M_Z, G_F\}$ and $\{\alpha(0), M_Z, G_F\}$ input schemes, along with the EW precision observables (EWPOs),¹

$$\alpha, \Gamma_W(\text{total}), \Gamma_Z(\text{total}), R_e, R_\mu, R_\tau, R_c, \sigma(\text{had}), A_\mu, A_\tau, A_s, A_c, A_b, A_{FB}^e, A_{FB}^\tau, A_{FB}^s, A_{FB}^c, A_{FB}^b. \quad (5)$$

These results are particularly useful for deriving sensitivities at a future Tera-Z facility [10–12].

For completeness, we also include results for $e^+e^- \rightarrow ZH$ [13, 14]. We include both polarized and unpolarized results at $\sqrt{s} = 240, 365, \text{ and } 500 \text{ GeV}$ with renormalization scales $\mu = \sqrt{s}$ and $\mu = 1 \text{ TeV}$.

¹In the $\{M_W, M_Z, G_F\}$ input scheme, M_W is replaced by α in Eq. (5). Definitions of the observables can be found in [11].

3 Results

3.1 Higgs Decays

We parameterize the Higgs decay widths and branching ratios as,

$$\frac{\Gamma(H \rightarrow X)^{(0,1)}}{\Gamma(H \rightarrow X)_{\text{SM}}} = 1 + \sum_i \delta_i^{(0,1)} C_i \quad (6)$$

$$\frac{BR(H \rightarrow X)^{(0,1)}}{BR(H \rightarrow X)_{\text{SM}}} = 1 + \sum_i \Delta_i^{(0,1)} C_i \quad (7)$$

where Γ_{SM} and $BR(H \rightarrow X)_{\text{SM}}$ are the world's best theory calculations taken from [17], the superscripts (0, 1) denote a LO or NLO result, respectively, and we have absorbed the factor of $\frac{1}{\Lambda^2}$ into the definition of $C_i \equiv \frac{\hat{C}_i^{(6)}}{\Lambda^2}$. We take a renormalization scale $\mu = m_H$ and set $\Lambda = 1$ TeV. For the remaining inputs, we use

$$\begin{aligned} M_W &= 80.352 \text{ GeV} & m_t &= 172.76 \text{ GeV} \\ M_Z &= 91.1535 \text{ GeV} & \alpha_S(m_h) &= 0.1188 \\ G_\mu &= 1.16638 \times 10^{-5} \text{ GeV}^{-2} & \Delta\alpha_{\text{had}}^{(5)} &= 0.02768, \\ m_H &= 125.1 \text{ GeV} \end{aligned} \quad (8)$$

where the W and Z masses correspond to experimental values $M_W^{\text{exp}} = 80.379$ GeV and $M_Z^{\text{exp}} = 91.1876$ GeV, rescaled using the pole definitions

$$M_V = \frac{M_V^{\text{exp}}}{\sqrt{1 + (\Gamma_V^{\text{exp}}/M_V^{\text{exp}})^2}}, \quad (9)$$

where $\Gamma_W^{\text{exp}} = 2.085$ GeV and $\Gamma_Z^{\text{exp}} = 2.495$ GeV. For $H \rightarrow f\bar{f}$ decays where light fermion masses are included, we take as inputs the on-shell (OS) and $\overline{\text{MS}}$ quark masses,

$$\begin{aligned} m_\tau &= 1.777 \text{ GeV} & m_\mu &= 0.1057 \text{ GeV} \\ m_b^{\text{OS}} &= 4.92 \text{ GeV} & m_b^{\overline{\text{MS}}}(m_b) &= 4.183 \text{ GeV} \\ m_c^{\text{OS}} &= 1.51 \text{ GeV} & m_c^{\overline{\text{MS}}}(m_c) &= 1.273 \text{ GeV} \\ m_s^{\text{OS}} &= 0.1 \text{ GeV}, & m_s^{\overline{\text{MS}}}(2 \text{ GeV}) &= 0.0935 \text{ GeV}. \end{aligned} \quad (10)$$

where the $\overline{\text{MS}}$ quark masses are run to $\mu = m_H$ using DSIXTOOLS [18, 19]. For $H \rightarrow 4f$, we compute the full four-body final state at LO, while in the NLO correction we use the narrow width approximation, $H \rightarrow f_{g_1}\bar{f}_{g_1}V$, $V \rightarrow f_{g_2}\bar{f}_{g_2}$. Inclusive numerical values for δ_i and Δ_i are in the POPxf files.

For $H \rightarrow q\bar{q}$, the choice of the on-shell vs $\overline{\text{MS}}$ renormalization scheme for quark masses can have a sizable impact on the numerical results, depending on the operator. We show in Figs. 1 and 1 an example of this scheme dependence for $C_{\phi D}$ and $C_{d\phi}$ [3, 3]. The dependence on $C_{\phi D}$ has sizable cancellations at LO, making the difference between LO and NLO larger than for most other coefficients. For many operators, the scheme dependence on the quark masses is negligible, as seen in Fig. 2 and in Fig. 3 for $C_{\phi G}$. Since $H \rightarrow b\bar{b}$ is the largest branching ratio, this scheme dependence translates into scheme dependence of all branching ratios when expanding the denominator, as we show in Figs. 4, 5 and 6. Both mass renormalization schemes are included as separate POPxf files.

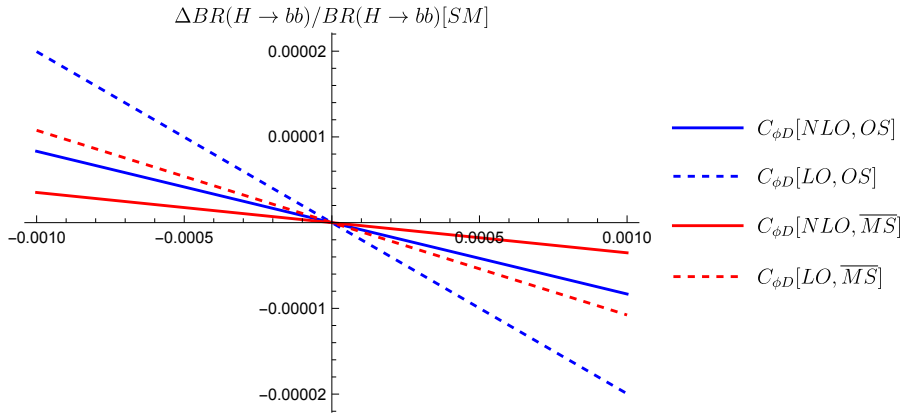


Figure 1: SMEFT contributions to the branching ratio of Higgs decay to $b\bar{b}$ normalized to the best SM value. The input scheme is $\{M_W, M_Z, G_F\}$, with a comparison of on-shell and $\overline{\text{MS}}$ renormalization of the masses.

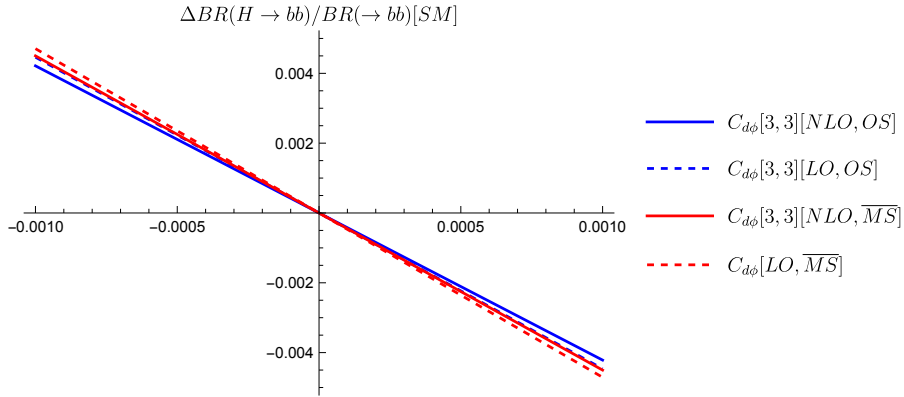


Figure 2: SMEFT contributions to the branching ratio of Higgs decay to $b\bar{b}$ normalized to the best SM value. The input scheme is $\{M_W, M_Z, G_F\}$, with a comparison of on-shell and $\overline{\text{MS}}$ renormalization of the masses.

An example of the $H \rightarrow e^+e^-\mu^+\mu^-$ branching ratio is shown in Fig. 7 for the $C_{\phi WB}$ contribution which appears at LO and we see a modest shift at NLO. The $C_{\phi \square}$ contribution 8 illustrates the dependence on the mass renormalization scheme.

For $H \rightarrow 4\ell$, we include files with a cut of $M_{Z^*} > 12$ GeV motivated by experimental analyses [20–22]. Here we define $M_{Z^{\ell\ell}}$ to be the same-flavour opposite sign lepton pair with invariant mass $M_{\ell\ell}$ closest to M_Z , and M_{Z^*} the opposite lepton pair. We also include results for $d\Gamma/dM_{Z^*}$ differential distributions for $H \rightarrow e^+e^-e^+e^-$, $H \rightarrow e^+e^-\mu^+\mu^-$, and $H \rightarrow \mu^+\mu^-\mu^+\mu^-$. We illustrate these results in Figs. 9 and 10 for a few select coefficients.²

For further details of the NLO calculation for all of the $H \rightarrow X$ processes including renormalization, IR subtraction, and a discussion of the validity of the narrow width approximation, we refer to the original publication [8] as well as the README at the GitLab repository [16].

3.2 Electroweak Observables

We have included NLO QCD and EW results for EWPOs, which provide significant constraints on dimension-6 global SMEFT fits, in the POPxf format. All 2-body decays of Z and W bosons

²Note that in the $M_{Z^*} > 12$ GeV inclusive results as well as the $d\Gamma/dM_{Z^*}$ differential distributions we use our own NLO SM calculation rather than a world’s best calculation.

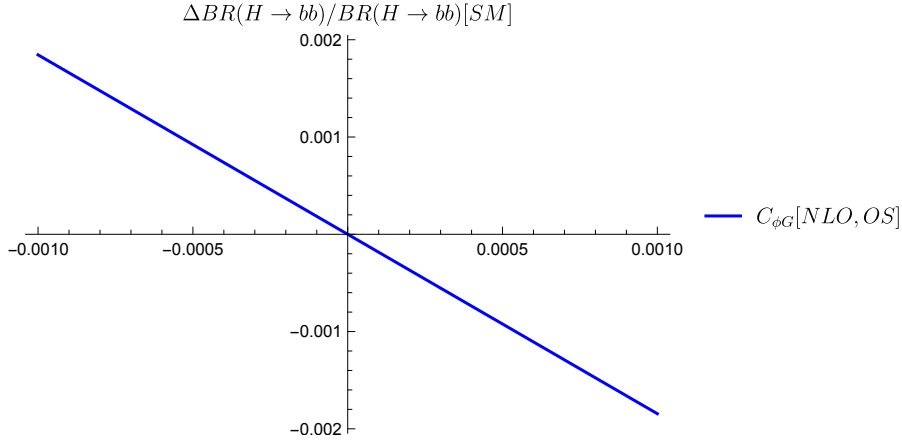


Figure 3: SMEFT contribution to the branching ratio of Higgs decay to $b\bar{b}$ normalized to the best SM value. The input scheme is $\{M_W, M_Z, G_F\}$. $C_{\phi G}$ enters only through its contribution to the total width and the LO and NLO curves are indistinguishable.

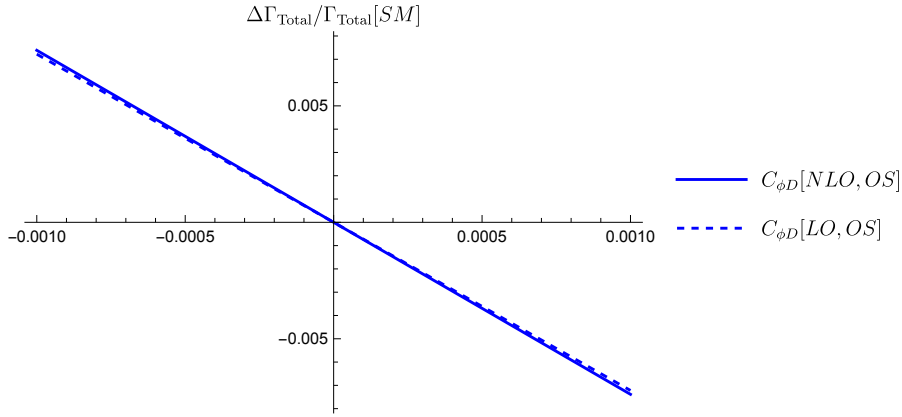


Figure 4: SMEFT contributions to the total Higgs width normalized to the best SM value. The LO and NLO $C_{\phi D}$ results are indistinguishable, as are the OS and \overline{MS} curves (not shown here).

at NLO are known to linear order in the dimension-6 SMEFT, with no assumptions on the flavor structure, allowing the construction of the EWPOs.

The input scheme dependence is known to be sizable for some operators. We have upgraded the results of [10] to include both the $\{\alpha(0), M_Z, G_F\}$ and $\{M_W, M_Z, G_F\}$ input schemes. Other possible input schemes such as $\{\alpha(M_Z), M_Z, G_F\}$ or $\{G_F, \sin\theta_{eff}^l, M_Z\}$ can be found in [12, 23]. We show in Figs. 11-19 results in different input schemes for some select coefficients where the difference between schemes is particularly large, using analogous notation to Eq. (7). The numerical values of the input parameters are given in the POPxf files. Figs. 11 and 12 show the contributions to the total Z width that are proportional to $C_{\phi D}$ and $C_{\phi WB}$ normalized to the most accurate theoretical prediction. $C_{\phi D}$ and $C_{\phi WB}$ contribute at tree level and the NLO results do not differ significantly from the LO results. There is, however, a significant input scheme dependence. The results for $C_{lq}^{(3)}$, which does not contribute at tree level, have a significantly smaller scheme dependence as seen in 13. Figs. 14-15 demonstrate that unlike the total width, the dependence of R_e shifts slightly going from LO to NLO for $C_{\phi D}$ and $C_{\phi WB}$ and there is a significant scheme dependence that persists at NLO. The scheme dependence of R_e proportional to $C_{lq}^{(3)}$ shown in Fig. 16 is smaller. Similar conclusions can be drawn

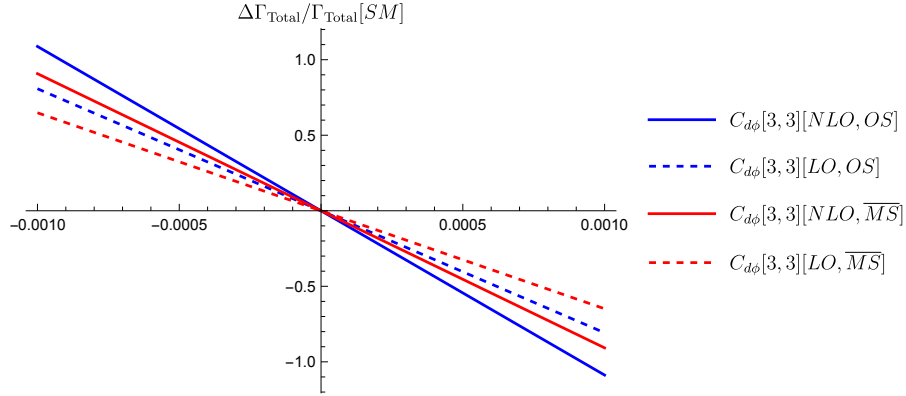


Figure 5: SMEFT contributions to the total Higgs width normalized to the best SM value. There small differences between OS and \overline{MS} renormalization.

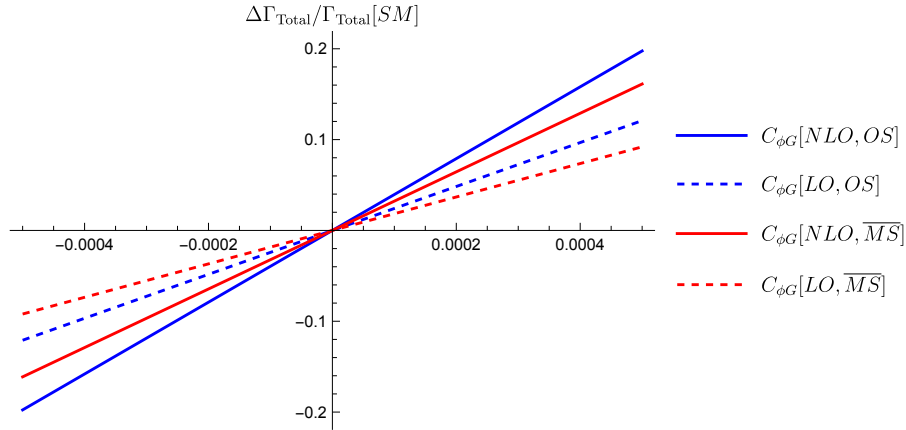


Figure 6: SMEFT contributions to the total Higgs width normalized to the best SM value and a comparison of OS and \overline{MS} renormalization.

from Figs. 17-173.

3.3 Higgstrahlung

SMEFT results for the total cross sections for $e^+e^- \rightarrow ZH$ at center-of-mass energies $\sqrt{s} = 240, 365$ and 500 GeV are also included as POPxf files using the calculations of [13, 14]. Both polarized and unpolarized results are presented. These files include the full LO and NLO SMEFT results including both QCD and electroweak corrections. The QED corrections can be found independently in [13, 14] if needed. The SMEFT contributions include all dimension-6 operators with no restrictions on the flavor structures and are accurate to linear order, $\mathcal{O}(\frac{1}{\Lambda^2})$, in the SMEFT expansion. The arbitrary renormalization scale arising at NLO, μ , is set to either $\mu = 1$ TeV or $\mu = \sqrt{s}$ and the input parameters are taken to be M_W, M_Z and G_F .

4 Conclusion

Global fits to SMEFT parameters provide an important source of information about potential high scale physics. Measurements of Higgs decays and Z-pole observables are crucial components of these fits. We have compiled results [16] that are accurate to linear order in the dimension-6 SMEFT and to NLO QCD and electroweak order for all 2- and 4- body Higgs de-

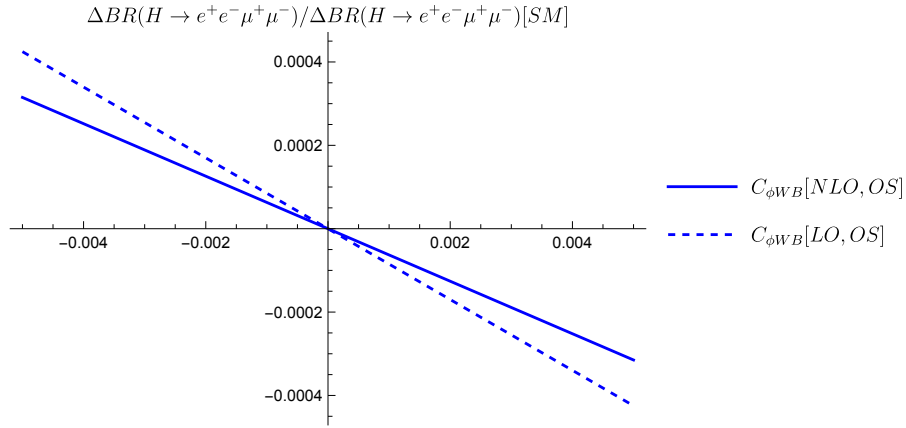


Figure 7: SMEFT contribution to branching ratio $H \rightarrow e^+e^-\mu^+\mu^-$. LHS: The curves with OS and \overline{MS} renormalization are indistinguishable.

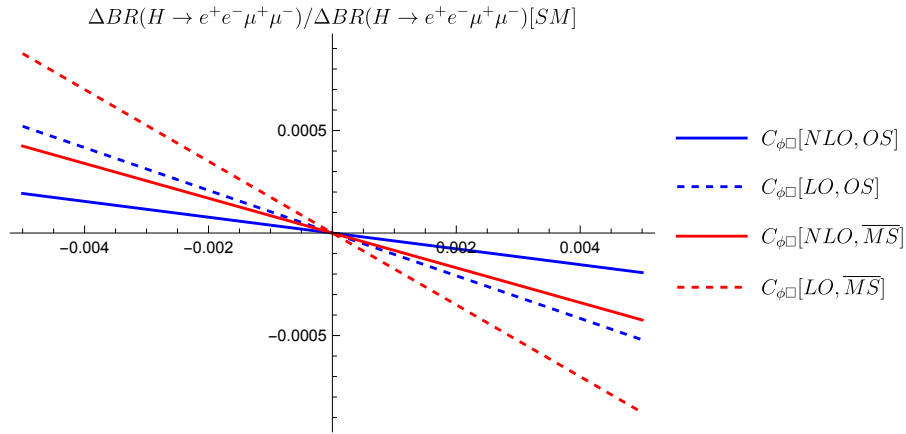


Figure 8: SMEFT contribution to branching ratio $H \rightarrow e^+e^-\mu^+\mu^-$.

cays and for all 2-body Z-pole decays using the POPxf data structure. These results can be straightforwardly implemented into global fits and experimental codes. For completeness, we have also presented NLO SMEFT results for $e^+e^- \rightarrow ZH$ in the POPxf format.

The eventual goal of the dimension-6 NLO QCD/EW SMEFT program is to have all the ingredients required to perform global fits consistently at NLO. At the LHC, most SMEFT predictions for production processes are currently available at NLO QCD accuracy, but not yet at full NLO EW precision. The results presented here therefore constitute an essential ingredient for future LHC fits at complete dimension-6 NLO QCD/EW accuracy. At the future FCC-ee, the Higgs decay results of this work can already be combined with calculations of the Higgstrahlung process and precision Z-pole observables to perform fits consistently at NLO QCD/EW order. In this setting, the POPxf formalism can play an important role by providing a common interface for the implementation and exchange of precision SMEFT predictions, making it easier to combine results from different calculations within global analyses.

Acknowledgements

S.D. and C.D.P. are supported by the U.S. Department of Energy under Contract No. DE-SC0012704. P.P.G. is supported by the Ramón y Cajal grant RYC2022-038517-I funded by

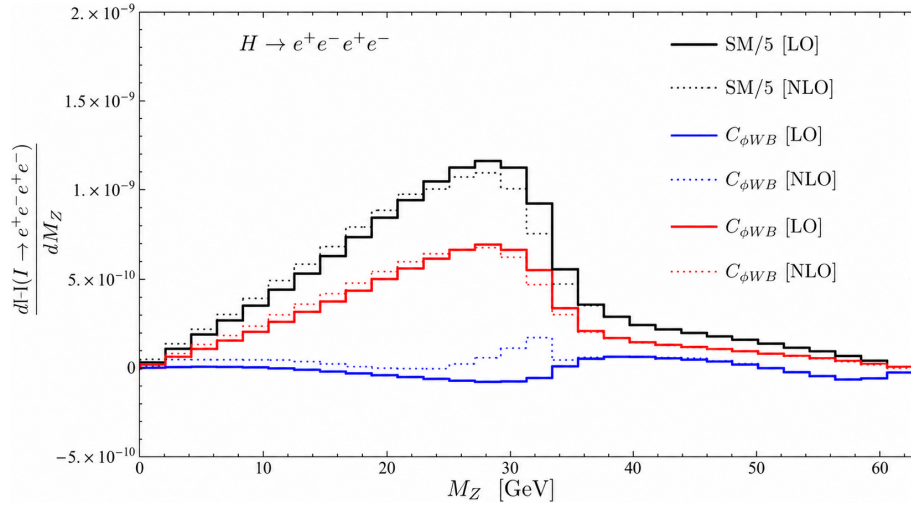


Figure 9: SMEFT contributions to the $d\Gamma/dM_{Z^*}$ differential distributions for $H \rightarrow e^+e^-\mu^+\mu^-$.

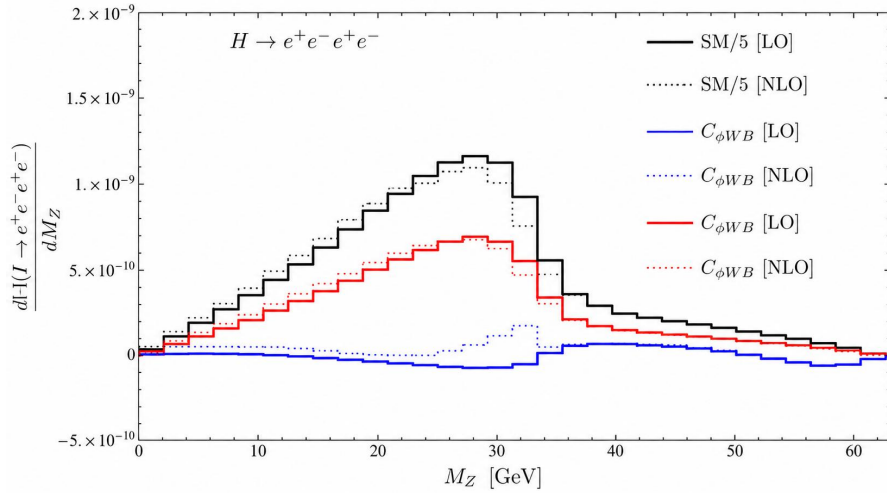


Figure 10: SMEFT contributions to the $d\Gamma/dM_{Z^*}$ differential distributions for $H \rightarrow e^+e^-e^+e^-$.

MCIN/AEI/10.13039/501100011033 and by FSE+, and by the Spanish Research Agency (Agencia Estatal de Investigación) through the grant IFT Centro de Excelencia Severo Ochoa No CEX2020-001007-S. The work of L.B. is supported in part by the U.S. Department of Energy under Grant No. DE-SC0010102 and by the College of Arts and Sciences of Florida State University. L.B. thanks the Technische Universität München (TUM) for the hospitality and the Excellence Cluster ORIGINS which is funded by the Deutsche Forschungsgemeinschaft (DFG, German Research Foundation) under Germany's Excellence Strategy – EXC-2094 – 390783311 for partial support during the completion of this work. Digital data in the POPxf format is provided at a [GitLab](#) repository.

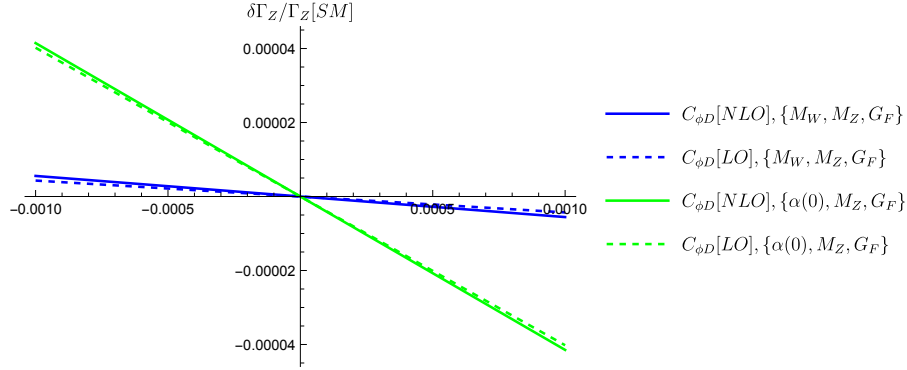


Figure 11: Results for Γ_Z proportional to $C_{\phi D}$ at LO and NLO in different input schemes normalized to the most accurate theoretical prediction.

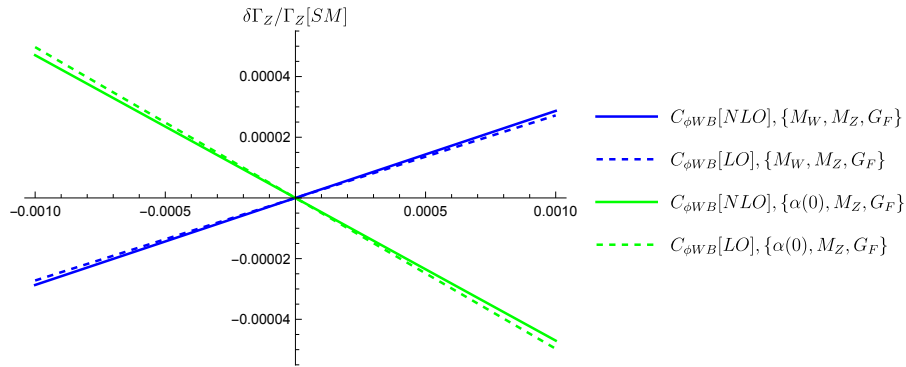


Figure 12: Results for Γ_Z proportional to $C_{\phi WB}$ at LO and NLO in different input schemes normalized to the most accurate theoretical prediction.

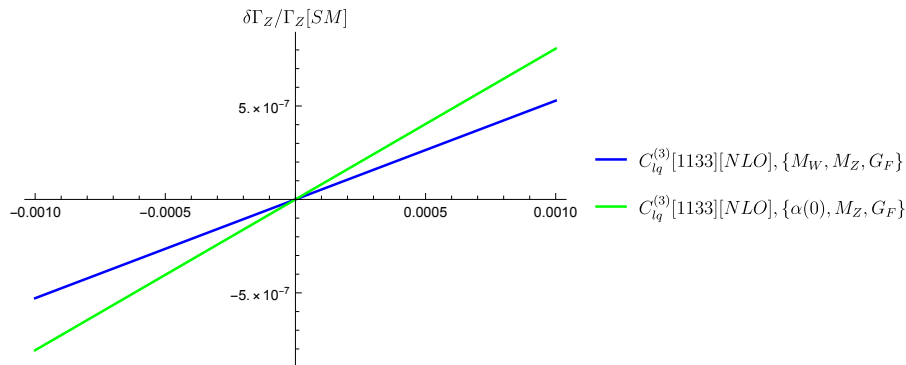


Figure 13: Results for Γ_Z proportional to $C_{lq}^{(3)}$ at LO and NLO in different input schemes normalized to the most accurate theoretical prediction.

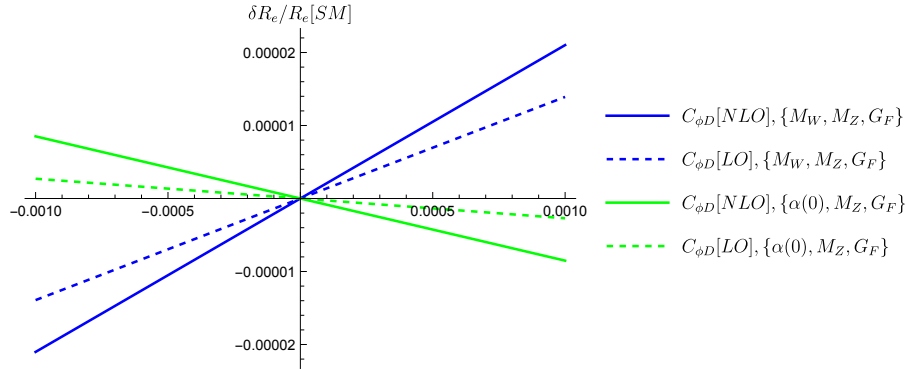


Figure 14: Results for R_e proportional to $C_{\phi D}$ at LO and NLO in different input schemes normalized to the most accurate theoretical prediction.

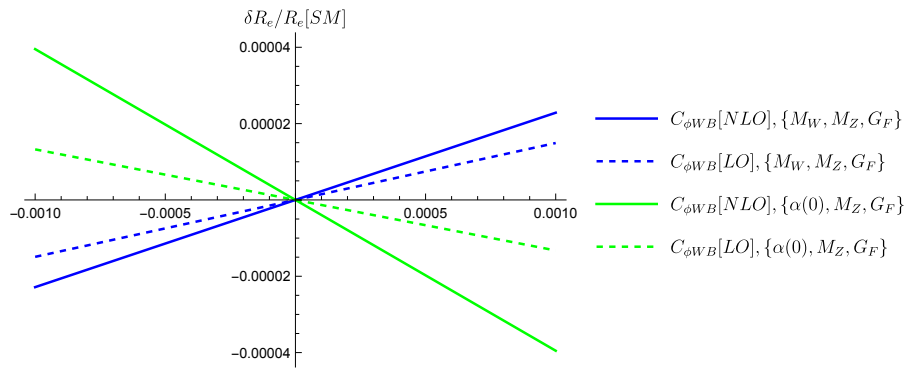


Figure 15: Results for R_e proportional to $C_{\phi WB}$ at LO and NLO in different input schemes normalized to the most accurate theoretical prediction.

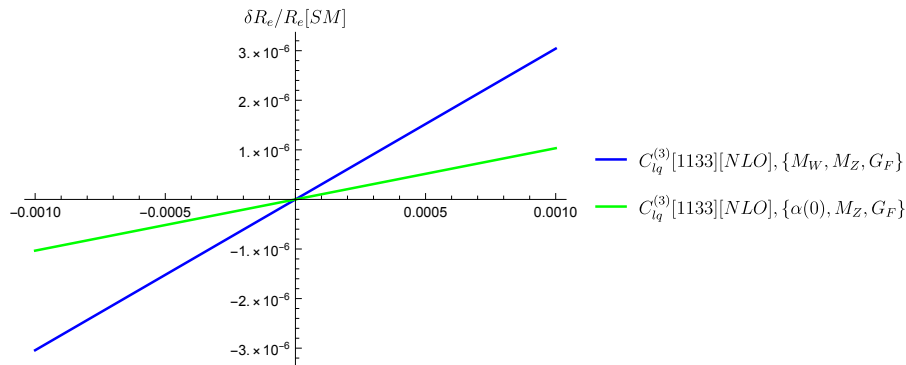


Figure 16: Results for R_e proportional to $C_{lq}^{(3)}$ at LO and NLO in different input schemes normalized to the most accurate theoretical prediction.

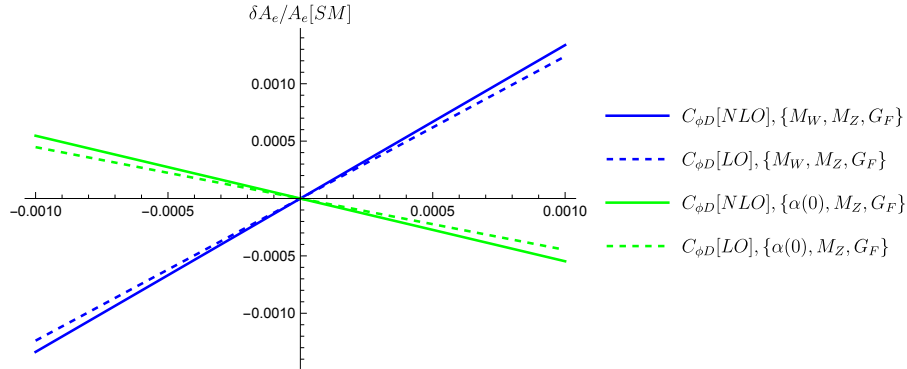


Figure 17: Results for A_e proportional to $C_{\phi D}$ at LO and NLO in different input schemes normalized to the most accurate theoretical prediction.

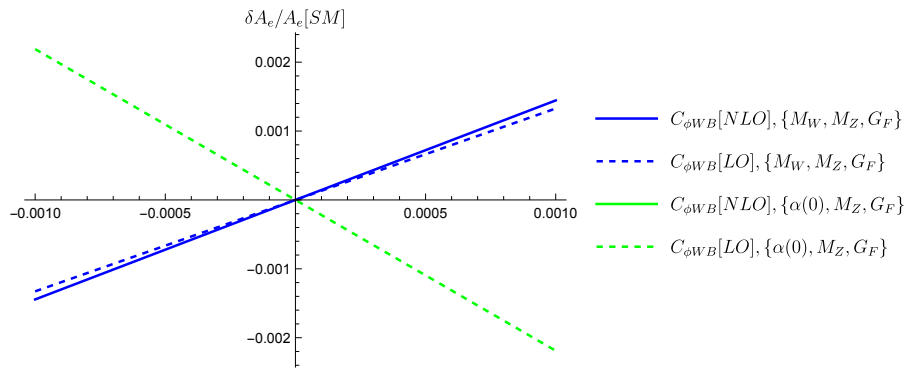


Figure 18: Results for A_e proportional to $C_{\phi WB}$ at LO and NLO in different input schemes normalized to the most accurate theoretical prediction.

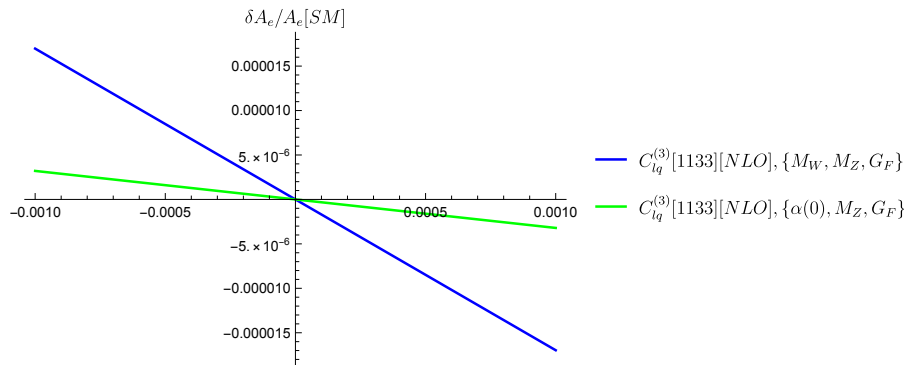


Figure 19: Results for A_e proportional to $C_{lq}^{(3)}$ at LO and NLO in different input schemes normalized to the most accurate theoretical prediction.

References

- [1] I. Brivio and M. Trott, *The Standard Model as an Effective Field Theory*, Phys. Rept. **793**, 1 (2019), doi:[10.1016/j.physrep.2018.11.002](https://doi.org/10.1016/j.physrep.2018.11.002), [1706.08945](https://arxiv.org/abs/1706.08945).
- [2] B. Grzadkowski, M. Iskrzynski, M. Misiak and J. Rosiek, *Dimension-Six Terms in the Standard Model Lagrangian*, JHEP **10**, 085 (2010), doi:[10.1007/JHEP10\(2010\)085](https://doi.org/10.1007/JHEP10(2010)085), [1008.4884](https://arxiv.org/abs/1008.4884).
- [3] A. Dedes, W. Materkowska, M. Paraskevas, J. Rosiek and K. Suxho, *Feynman rules for the Standard Model Effective Field Theory in R_ξ -gauges*, JHEP **06**, 143 (2017), doi:[10.1007/JHEP06\(2017\)143](https://doi.org/10.1007/JHEP06(2017)143), [1704.03888](https://arxiv.org/abs/1704.03888).
- [4] J. Alwall, R. Frederix, S. Frixione, V. Hirschi, F. Maltoni, O. Mattelaer, H. S. Shao, T. Stelzer, P. Torrielli and M. Zaro, *The automated computation of tree-level and next-to-leading order differential cross sections, and their matching to parton shower simulations*, JHEP **07**, 079 (2014), doi:[10.1007/JHEP07\(2014\)079](https://doi.org/10.1007/JHEP07(2014)079), [1405.0301](https://arxiv.org/abs/1405.0301).
- [5] I. Brivio, *SMEFTsim 3.0 — a practical guide*, JHEP **04**, 073 (2021), doi:[10.1007/JHEP04\(2021\)073](https://doi.org/10.1007/JHEP04(2021)073), [2012.11343](https://arxiv.org/abs/2012.11343).
- [6] C. Degrande, G. Durieux, F. Maltoni, K. Mimasu, E. Vryonidou and C. Zhang, *Automated one-loop computations in the standard model effective field theory*, Phys. Rev. D **103**(9), 096024 (2021), doi:[10.1103/PhysRevD.103.096024](https://doi.org/10.1103/PhysRevD.103.096024), [2008.11743](https://arxiv.org/abs/2008.11743).
- [7] I. Brivio, K. Mimasu, P. Stangl, A. Biekötter, A. R. C. Gómez, C. Knight, L. Mantani, E. Rossi, A. N. Rossia and A. Smolkovič, *POPxf: An Exchange Format for Polynomial Observable Predictions* (2025), [2511.17348](https://arxiv.org/abs/2511.17348).
- [8] L. Bellafronte, S. Dawson, C. Del Pio, M. Forsslund and P. P. Giardino, *Higgs Decays at NLO in the SMEFT* (2026), [2601.09599](https://arxiv.org/abs/2601.09599).
- [9] L. Bellafronte, S. Dawson, C. Del Pio, M. Forsslund and P. P. Giardino, *Complete Next-to-Leading-Order Standard-Model-Effective-Field-Theory Electroweak Corrections to Higgs Decays*, Phys. Rev. Lett. **136**(5), 051801 (2026), doi:[10.1103/2wqp-5zfm](https://doi.org/10.1103/2wqp-5zfm), [2508.14966](https://arxiv.org/abs/2508.14966).
- [10] L. Bellafronte, S. Dawson and P. P. Giardino, *The importance of flavor in SMEFT Electroweak Precision Fits*, JHEP **05**, 208 (2023), doi:[10.1007/JHEP05\(2023\)208](https://doi.org/10.1007/JHEP05(2023)208), [2304.00029](https://arxiv.org/abs/2304.00029).
- [11] S. Dawson and P. P. Giardino, *Electroweak and QCD corrections to Z and W pole observables in the standard model EFT*, Phys. Rev. D **101**(1), 013001 (2020), doi:[10.1103/PhysRevD.101.013001](https://doi.org/10.1103/PhysRevD.101.013001), [1909.02000](https://arxiv.org/abs/1909.02000).
- [12] A. Biekötter and B. D. Pecjak, *Analytic results for electroweak precision observables at NLO in SMEFT*, JHEP **07**, 134 (2025), doi:[10.1007/JHEP07\(2025\)134](https://doi.org/10.1007/JHEP07(2025)134), [2503.07724](https://arxiv.org/abs/2503.07724).
- [13] K. Asteriadis, S. Dawson, P. P. Giardino and R. Szafron, *Impact of Next-to-Leading-Order Weak Standard-Model-Effective-Field-Theory Corrections in $e^+e^- \rightarrow ZH$* , Phys. Rev. Lett. **133**(23), 231801 (2024), doi:[10.1103/PhysRevLett.133.231801](https://doi.org/10.1103/PhysRevLett.133.231801), [2406.03557](https://arxiv.org/abs/2406.03557).
- [14] K. Asteriadis, S. Dawson, P. P. Giardino and R. Szafron, *$e^+e^- \rightarrow ZH$ process in the SMEFT beyond leading order*, JHEP **02**, 162 (2025), doi:[10.1007/JHEP02\(2025\)162](https://doi.org/10.1007/JHEP02(2025)162), [2409.11466](https://arxiv.org/abs/2409.11466).

- [15] L. Bellafronte, S. Dawson, C. Del Pio, M. Forsslund and P. P. Giardino, *NEWiSH: NLO ElectroWeak in the SMEFT for Higgs widths*, <https://gitlab.com/mforsslund/newish> (2025).
- [16] L. Bellafronte, S. Dawson, C. Del Pio, M. Forsslund and P. P. Giardino, *NLO SMEFT POPxf Results*, <https://gitlab.com/mforsslund/smeft-nlo-popxf> (2026).
- [17] D. de Florian *et al.*, *Handbook of LHC Higgs Cross Sections: 4. Deciphering the Nature of the Higgs Sector*, CERN Yellow Rep. Monogr. **2**, 1 (2017), doi:[10.23731/CYRM-2017-002](https://doi.org/10.23731/CYRM-2017-002), [1610.07922](https://arxiv.org/abs/1610.07922).
- [18] A. Celis, J. Fuentes-Martin, A. Vicente and J. Virto, *DsixTools: The Standard Model Effective Field Theory Toolkit*, Eur. Phys. J. C **77**(6), 405 (2017), doi:[10.1140/epjc/s10052-017-4967-6](https://doi.org/10.1140/epjc/s10052-017-4967-6), [1704.04504](https://arxiv.org/abs/1704.04504).
- [19] J. Fuentes-Martin, P. Ruiz-Femenia, A. Vicente and J. Virto, *DsixTools 2.0: The Effective Field Theory Toolkit*, Eur. Phys. J. C **81**(2), 167 (2021), doi:[10.1140/epjc/s10052-020-08778-y](https://doi.org/10.1140/epjc/s10052-020-08778-y), [2010.16341](https://arxiv.org/abs/2010.16341).
- [20] G. Aad *et al.*, *Measurement of the $H \rightarrow \gamma\gamma$ and $H \rightarrow ZZ^* \rightarrow 4\ell$ cross-sections in pp collisions at $\sqrt{s} = 13.6$ TeV with the ATLAS detector*, Eur. Phys. J. C **84**(1), 78 (2024), doi:[10.1140/epjc/s10052-023-12130-5](https://doi.org/10.1140/epjc/s10052-023-12130-5), [2306.11379](https://arxiv.org/abs/2306.11379).
- [21] V. Chekhovsky *et al.*, *Measurements of the Higgs boson production cross section in the four-lepton final state in proton-proton collisions at $\sqrt{s} = 13.6$ TeV*, JHEP **05**, 079 (2025), doi:[10.1007/JHEP05\(2025\)079](https://doi.org/10.1007/JHEP05(2025)079), [2501.14849](https://arxiv.org/abs/2501.14849).
- [22] S. Dawson, M. Forsslund and P. P. Giardino, *NLO SMEFT electroweak corrections to Higgs boson decays to four leptons in the narrow width approximation*, Phys. Rev. D **111**(1), 015016 (2025), doi:[10.1103/PhysRevD.111.015016](https://doi.org/10.1103/PhysRevD.111.015016), [2411.08952](https://arxiv.org/abs/2411.08952).
- [23] A. Biekötter, B. D. Pecjak and T. Smith, *Using the effective weak mixing angle as an input parameter in SMEFT*, JHEP **04**, 073 (2024), doi:[10.1007/JHEP04\(2024\)073](https://doi.org/10.1007/JHEP04(2024)073), [2312.08446](https://arxiv.org/abs/2312.08446).